Supplementary Information

Purely electronic insulator-metal transition in rutile VO_2

Shaobo Cheng *et al.*

*Corresponding author. Email: zhu@bnl.gov

Supplementary Text

Section S1-Electron energy loss spectroscopy (EELS) calculation methods

For the $CdS/VO_2/TiO_2$ system, valence EELS line scans were performed. Each EELS was deconvoluted using the Fourier-log method to remove the zero-loss peak and multiple scattering, and then the dielectric function was retrieved. These processes were completed by using the DigitalMicrograph software. The details of these processes can be found in chapter 4 of Ref [1].

With the acquired EELS spectra, the dielectric functions can be retrieved. Considering the Jellium model for the plasmons, the imaginary part of dielectric function ε is described as (1):

$$Im[\frac{-1}{\varepsilon(\omega)}] = \frac{\omega\Gamma\omega_P^2}{(\omega^2-\omega_P^2)^2+(\omega\Gamma)^2} \quad (1)$$

where ω_P is the resonant frequency of the plasma oscillation and will generate a quasi-particle with the energy of $E_P = \hbar\omega_P$, Γ is damping constant for the plasma in Drude model. Similarly, Function (1) can be written as:

$$Im[\frac{-1}{\varepsilon(E)}] = \frac{E_P^2(E\hbar/\tau)}{(E^2-E_P^2)^2+(E\hbar/\tau)^2} = \frac{E(\Delta E_P)E_P^2}{(E^2-E_P^2)^2+(E\Delta E_P)^2} \quad (2)$$

where $\tau = \frac{1}{\Gamma}$, E is the energy read from EELS, E_P is the peak position for plasmons.

According to the Kramers-Kronig relationship:

$$Re[\frac{1}{\varepsilon(E)}] = 1 - \frac{2}{\pi}P\int_0^\infty Im[\frac{-1}{\varepsilon(E')}]\frac{E'dE'}{E'^2-E^2} \quad (3)$$

where P is Cauchy spindle integral (excluding $E = E'$).

Thus, the dielectric function can be expressed as:

$$\varepsilon(E) = \varepsilon_1(E) + i\varepsilon_2(E) = \frac{Re[1/\varepsilon(E)]+i\,Im[-1/\varepsilon(E)]}{\{Re[1/\varepsilon(E)]\}^2+\{Im[-1/\varepsilon(E)]\}^2} \quad (4)$$

To calculate the EELS spectra with the dielectric function, the formula is shown as:

$$\frac{\partial^2 I}{\partial E\partial q} = \frac{2}{\pi a_0 m v^2 n_a}\mathrm{Im}\left[-\frac{1}{\varepsilon(q,E)}\right]\frac{dq}{q} \quad (5)$$

where $a_0 = 4\pi\varepsilon_0\hbar^2/m_0e^2$ (first Bohr radius), n_a is the number of atoms per unit volume, v is the speed of incident electrons, q is momentum transfer.

The energy of plasma peak (E, *i.e.,* the position of the highest plasma peak) and plasma frequency (ω_p) in semiconductors or insulators are: [2-4]

$$E = \hbar\omega_p \quad (6)$$

$$\omega_p^2 = \frac{4\pi e^2 N_{eff}}{m(1+\delta\varepsilon_0)} \quad (7)$$

where

$$N_{eff} = \frac{m}{m^*} N_v + \sum_{l>\upsilon} f_{l\upsilon} \quad (8)$$

e is the elementary charge; m and m^* are, respectively, the mass and effective mass of electrons; N_v is the number of valence electrons of intraband transition in the conduction band; the term $\sum_{l>v} f_{l\upsilon}$ in Equation (8) is the electron number transferred from the valence band v to the conduction band l. $\delta\varepsilon_0$ is a correction which comes from interband transitions of core shell electrons. $\delta\varepsilon_0$ is zero or near zero if the core shell bands are sufficiently far removed and uncoupled from the valence bands (4, 5), so $\delta\varepsilon_0$ was ignored in our calculation. As described in Eq. (8), plasma excitation is contributed by the conduction- and valence-band electrons. Their masses are, the effective(m*) and real mass respectively [4-6]. For VO_2, before illumination, the electrons contributing to the plasma oscillation arise from the valence bands. The electron mass is taken as the electron rest mass. During illumination, some electrons are kicked out of the valence bands. The intraband transition will occur in the valence bands, and affect the plasma excitation. To estimate the plasma peak, the intraband transition effective electron mass should be used. For simplicity, as an approximation the electron rest mass is used in our calculations.

All the previous simplifications lead to Eq. (9) and relate the bulk (or valence) plasmons frequency ω_p to the density of the valence electrons N_v. The Coulomb charge e and the mass of the electron m are similar to those in the free electron model.

$$\omega_p^2 = \frac{4\pi e^2 N_v}{m} \quad (9)$$

The change of electron density before and after light radiation can be written as

$$\Delta N = \frac{m}{4\pi e^2}[\omega_b^2 - \omega_a^2] \quad (10)$$

where ω_b and ω_a are bulk plasmon frequencies before and after illumination, respectively.

Using Eq. (10), the charge transfer at the interfaces of oxide thin films can be estimated. It is important to note that the free electron model is not sufficient to quantitatively capture the density of the free electrons of a strongly correlated material (such as VO_2). Nonetheless, since the VO_2 is not undergoing any phase transformation during illumination, the valence plasmons frequency change can be attributed to the change in the valence electron density.

Section S2-Time resolved light induced metal to insulator transition.

The hybrid system exhibits (quasi)nonvolatile behavior, characterized by its inability (in short time) to revert to its original state after exposure to light. In other words, even when the sample is measured without illumination, it maintains its altered state (as indicated by the green dashed line in Fig. S5). The inset graph (measured at 260 K) underscores the persistence of this change even after the excitation source has been removed. Given the 8 nm thickness of VO_2, we aim to restrict the temperature increase during the transition to the metallic state to below 360 K. In Fig. S6, the relaxation of the system after irradiating the sample with light has been measured. We stop at 320 K and wait at that temperature for 2 hours, then measure the metal-insulator transition (dashed blue lines). Subsequently, the system returns to 320 K and holds another 2 hours to verify if it continus relaxing and measure again (dot-dashed purple line). Afterwards, the system returns to 320 K and holds additional 2 hours (6 hours in total – small green dots), then measure the electrical transport. Finally, the system returns to 320 K and holds 2 more hours (8 hours – continuous red line), where we observe that it has recovered its original state. In Fig. S6(a), we have marked with green asterisks the resistance values at 270 K, which have been plotted in Fig. S6(b). Waiting at 320 K allows the system to relax much faster than if it were at 270 K. At higher temperatures (320 K), the thermal energy available to the system is greater than that at 270 K. This increased thermal energy facilitates faster relaxation processes, as it allows trapped carriers to leave the defect sites faster.

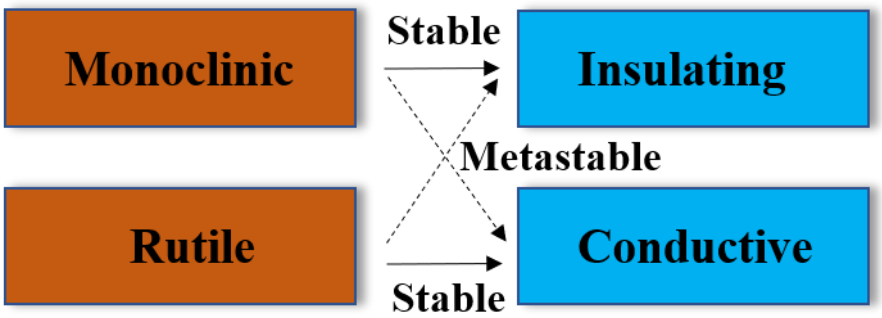

Fig. S1 Electronic-crystal structure phase diagram of VO_2. The monoclinic insulating phase and rutile conductive phase are two stable phases for VO_2, while the reported monoclinic conductive phase is a metastable phase. In this work, the rutile insulating phase has been explored.

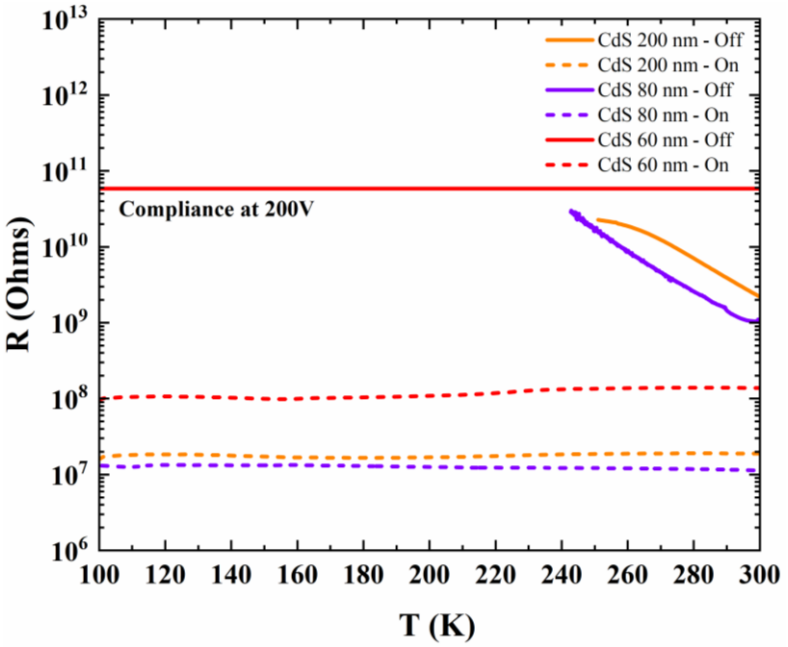

Fig. S2 Electrical transport measurements of the CdS semiconductor for different thicknesses as a function of temperature from 100–300 K. Continuous (dashed) lines represent the light off (on) condition. We see a trend towards higher resistivity for thinner films and a dramatic decrease in resistivity after illumination. The red continuous line (CdS – 60 nm) shows a temperature-independent resistance when using a compliance of 200 V, and dashed line under light, with resistance around 10^8 ohms.

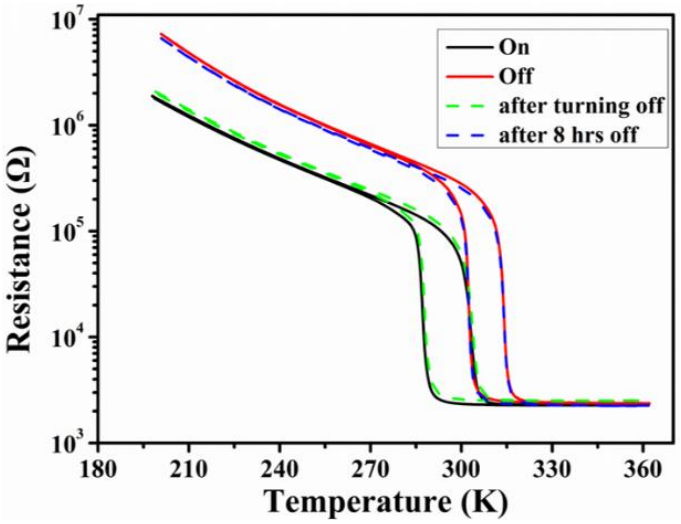

Fig. S3 Photo induced modification of the metal-insulator transition (MIT) of the $CdS/VO_2/TiO_2$ heterostructure. The red and black solid lines are resistance vs temperature for the pristine state (before shining light, light off state) and light on state, respectively. The dashed green and blue lines are the results measured immediately after turning the light off and after turning the light off for 8 hours, respectively.

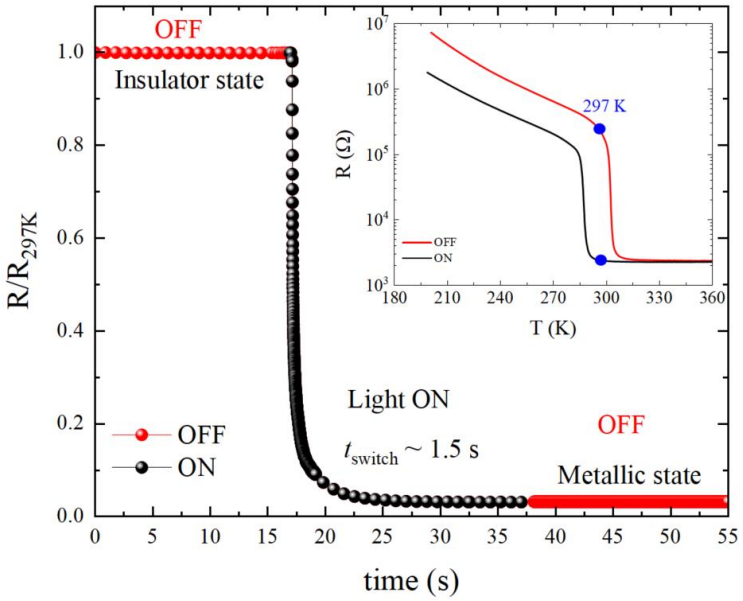

Fig. S4 Relaxation time of CdS/VO_2 normalized at 297 K. The red data points represent the original curve in the insulating state (refer to the inset, upper blue point at 297 K), while the black points represent the state when exposed to light at a power of 75 mW/cm^2. The transition time (t_{switch}) from the insulating to the metallic state is approximately 1.5 seconds. Alterations in electrical transport are illustrated in the inset using blue dots.

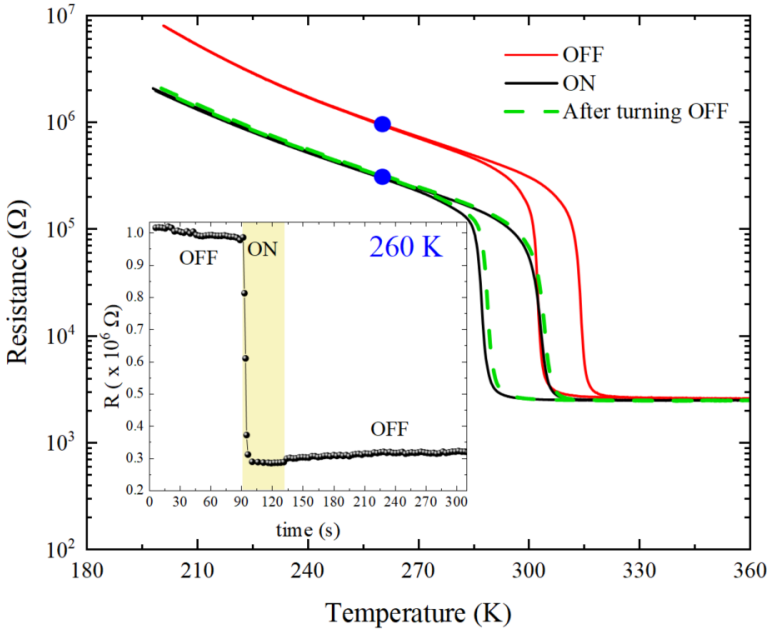

Fig. S5 Resistance as a function of temperature in CdS/VO_2. The green dashed curve represents the measurement of electrical transport conducted immediately after light exposure. In the insulating state at 260K, the resistance relaxation undergoes a permanent change after the light is removed.

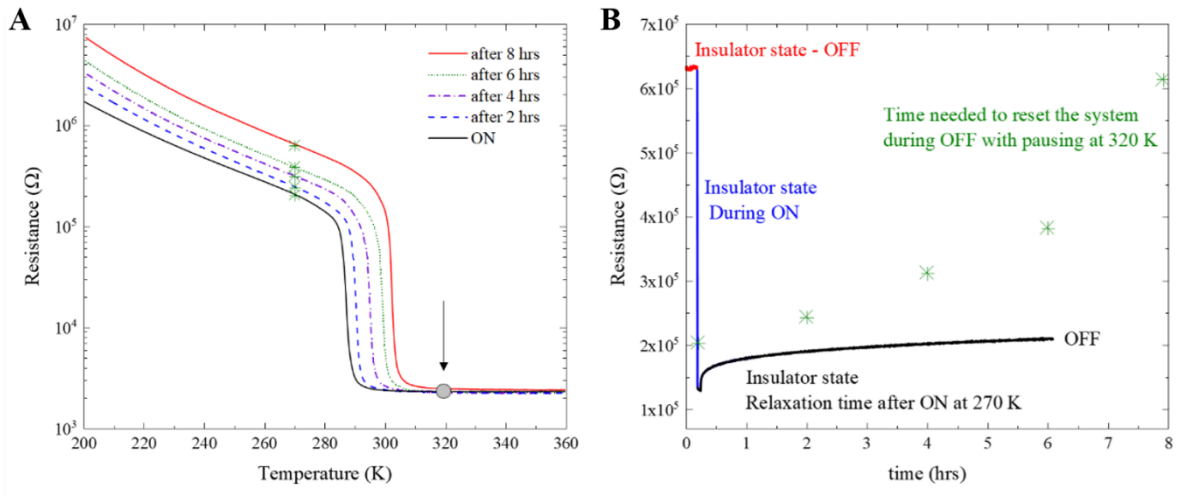

Fig. S6 (A) The system's relaxation after light irradiation is examined by repeatedly pausing at 320 K for progressively longer durations and measuring the metal-insulator transition. Measurements are taken after 2 hours (dashed blue line), 4 hours (dot-dashed purple line), 6 hours (small green dots), and 8 hours (continuous red line). By the 8-hour mark, the system has fully recovered its original state, as indicated by the electrical transport measurements. (B) Relaxation time at 270 K for 6 hours (continuous black line). Green asterisks correspond the relaxation of the system at 270 K including a pause at 320 K.

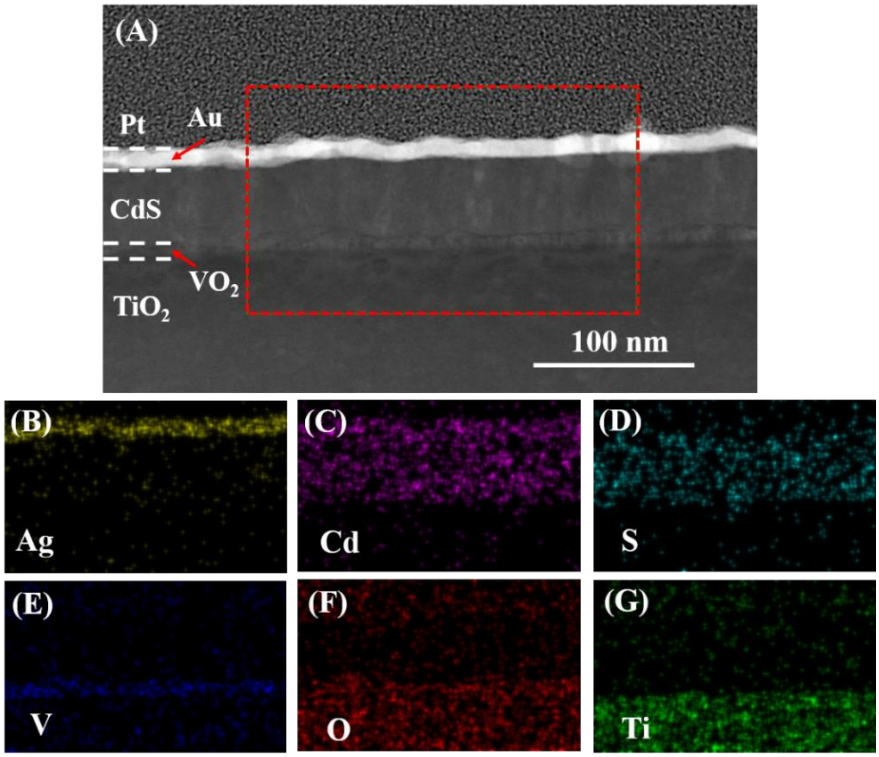

Fig. S7 Scanning transmission electron microscopy of the $CdS/VO_2/TiO_2$ heterostructure. (A) Low magnification high angle annular dark field (HAADF) STEM image of the $CdS/VO_2/TiO_2$ system. The EDS (energy dispersive spectroscopy) mapping was carried out in the red dashed rectangle area. (B)-(G) are EDS mapping of Ag, Cd, S, V, O, and Ti, respectively.

Section S3-DFT computational methods

Spin-polarized DFT [7, 8] calculations were performed using the Vienna Ab initio Simulation Package (VASP) [9, 10] within the projector augmented wave (PAW) [11] approach. The exchange-correlation effects were modeled using the Perdew-Burke-Ernzerhof (PBE) [12] generalized gradient approximations (GGA) [13] functional with a plane wave cutoff of 520 eV. The pseudopotentials were the same as in the Materials Project [14], where the core electrons were described with the frozen core approximation by the PAW potential, while the valence electrons of vanadium and oxygen are given by V: $3d^3\ 4s^2$ and O: $2s^2\ 2p^4$. The convergence criteria were set to 5×10^{-5} eV and -0.01 eV/Å for energies and atomic forces, respectively. Γ-centered *k*-point meshes of 11×11×6 were used for calculations. All input generation and analysis were performed with the Python Materials Genomics (pymatgen) library [15].

The initial tetragonal VO_2 crystal structure with space group *P4₂/mmm* was taken from the Materials Project. To better describe the transition metals in the oxides, the DFT + *U* method [16] was used for all calculations, with a Hubbard [17] parameter $U = 3.06$ eV for the V-*3d* orbital [18]. This U value results in a band gap of 0.6 eV for insulating low-temperature VO_2, which matches the experimental value [19]. Experimental lattice constants were applied to rutile VO_2 to match the experimental strain experienced by the system due to size mismatch from TiO_2. Hole doping was performed on the strained rutile phase by changing the total number of electrons in the unit cell with a compensating change in the jellium background charge.

Reference

1. Egerton, R.F. Electron Energy-Loss Spectroscopy in the Electron Microscope. (Springer New York, NY, 2011).
2. Mecklenburg, M. et al. Nanoscale temperature mapping in operating microelectronic devices. *Science* **347**, 629-632 (2015).
3. Rez, P. & Muller, D.A. The Theory and Interpretation of Electron Energy Loss Near-Edge Fine Structure. *Annual Review of Materials Research* **38**, 535-558 (2008).
4. Pines, D. Elementary Excitations in Solids. (W.A. Benjamin, New York; 1963).
5. Philipp, H.R. & Ehrenreich, H. Optical Properties of Semiconductors. *Physical Review* **129**, 1550-1560 (1963).
6. Meng, Q. et al. Quantification of Charge Transfer at the Interfaces of Oxide Thin Films. *The Journal of Physical Chemistry A* **123**, 4632-4637 (2019).

7. Hohenberg, P. & Kohn, W. Inhomogeneous Electron Gas. *Physical Review* **136**, B864-B871 (1964).
8. Kohn, W. & Sham, L.J. Self-Consistent Equations Including Exchange and Correlation Effects. *Physical Review* **140**, A1133-A1138 (1965).
9. Kresse, G. & Furthmüller, J. Efficient iterative schemes for ab initio total-energy calculations using a plane-wave basis set. *Physical Review B* **54**, 11169-11186 (1996).
10. Kresse, G. & Furthmüller, J. Efficiency of ab-initio total energy calculations for metals and semiconductors using a plane-wave basis set. *Computational Materials Science* **6**, 15-50 (1996).
11. Blöchl, P.E. Projector augmented-wave method. *Physical Review B* **50**, 17953-17979 (1994).
12. Perdew, J.P., Burke, K. & Ernzerhof, M. Generalized Gradient Approximation Made Simple. *Physical Review Letters* **77**, 3865-3868 (1996).
13. Perdew, J.P. et al. Atoms, molecules, solids, and surfaces: Applications of the generalized gradient approximation for exchange and correlation. *Physical Review B* **46**, 6671-6687 (1992).
14. Jain, A. et al. Commentary: The Materials Project: A materials genome approach to accelerating materials innovation. *APL Materials* **1**, 011002 (2013).
15. Ong, S.P. et al. Python Materials Genomics (pymatgen): A robust, open-source python library for materials analysis. *Computational Materials Science* **68**, 314-319 (2013).
16. Anisimov, V.I., Zaanen, J. & Andersen, O.K. Band theory and Mott insulators: Hubbard U instead of Stoner I. *Physical Review B* **44**, 943-954 (1991).
17. Himmetoglu, B., Floris, A., de Gironcoli, S. & Cococcioni, M. Hubbard-corrected DFT energy functionals: The LDA+U description of correlated systems. *International Journal of Quantum Chemistry* **114**, 14-49 (2014).
18. Cheng, S. et al. Inherent stochasticity during insulator-metal transition in VO2. *Proceedings of the National Academy of Sciences* **118**, e2105895118 (2021).
19. Zylbersztejn, A. & Mott, N.F. Metal-insulator transition in vanadium dioxide. *Physical Review B* **11**, 4383-4395 (1975).